JETIR.ORG ISSN: 2349-5162 | ESTD Year : 2014 | Monthly Issue
JOURNAL OF EMERGING TECHNOLOGIES AND INNOVATIVE RESEARCH (JETIR)
An International Scholarly Open Access, Peer-reviewed, Refereed Journal

Synthesis and Characterization of Perovskite Solar Cell

[1] Golla Naveen Kumar, [2] Dr. K. Srinivasa Reddy
[1 & 2] Department of Physics
[1 & 2] JNTUH College of Engineering, Science and Technology, Hyderabad-500085

ABSTRACT: Perovskite solar cells (PSCs) represent an advanced photovoltaic technology with promising potential for high efficiency and cost-effective energy production. This study explores the synthesis and characterization of PSCs with a focus on enhancing efficiency and stability. Using a spin-coating technique, perovskite layers were deposited on substrates, followed by detailed optical and structural characterization to evaluate properties such as crystallinity, light absorption, and thermal stability. The results indicate significant potential for efficiency improvements through optimized material composition and controlled processing parameters. Various configurations were assessed for their performance under real-world conditions, with specific attention to the durability and environmental impact of lead-based perovskites. The findings highlight that using certain electron transport layers can enhance device performance and longevity, while challenges such as lead toxicity and scalability need further research. These insights contribute to the ongoing efforts to make PSCs a commercially viable option for sustainable energy production.

KEYWORDS: Perovskite solar cell, $CsPbIBr_2$ Thin films, XRD Analysis, Annealing Temperature, Optical Properties

1. INTRODUCTION:

Perovskite solar cells (PSCs) have emerged as a game-changing technology in photovoltaic research, primarily due to their rapid advancements in efficiency and potential for low-cost production. Compared to conventional silicon-based solar cells, PSCs demonstrate several advantages, including strong light absorption across a wide spectral range, adjustable bandgaps, and long charge carrier diffusion lengths. These properties allow efficient energy conversion even with thin material layers, minimizing both material use and energy consumption during production.[1][2]

The adaptability of perovskite materials, which can be fabricated at relatively low temperatures and applied to flexible substrates, presents vast opportunities for various applications, such as in building-integrated photovoltaics and lightweight, portable energy solutions. However, there are still significant challenges that must be addressed before PSCs can be widely adopted. Key issues include the limited stability of perovskite materials when exposed to environmental factors like moisture, heat, and UV radiation, as well as concerns about the use of toxic lead compounds.[3][4]

This study investigates the synthesis and detailed characterization of PSCs, with an emphasis on overcoming these limitations. By exploring alternative materials, improved encapsulation methods, and scalable production techniques, this research seeks to enhance both the longevity and performance of PSCs, contributing to their potential for large-scale implementation in the renewable energy sector.[5][6]

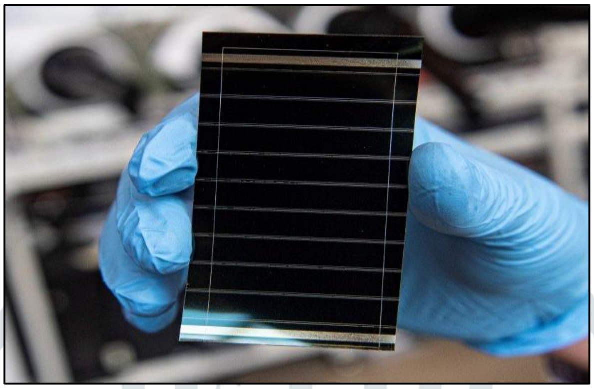

Figure 1: Structure of Perovskite Solar cell

1. EXPERIMENTAL METHOD:

Materials and Chemicals

Cesium iodide (CsI) and lead bromide ($PbBr_2$) were selected as the precursors for the synthesis of $CsPbIBr_2$ thin films. Dimethyl sulfoxide (DMSO) was utilized as the solvent in the precursor solution preparation, while isopropanol (IPA), acetone, and distilled water were employed as cleaning agents for substrate preparation.[7]

Substrate Cleaning

Proper substrate cleaning is essential to ensure a contaminant-free surface, which is critical for achieving uniform and high-quality thin films. Glass substrates were first immersed in detergent and ultrasonically cleaned for 5 minutes. This was followed by rinsing with distilled water to remove any detergent residues. The substrates were then sequentially soaked in IPA and acetone for 5–10 minutes each to remove organic contaminants. After cleaning, the substrates were dried at 60°C to eliminate any remaining moisture and were subsequently stored in IPA until the deposition process.[8]

Preparation of $CsPbIBr_2$ Precursor Solution

The $CsPbIBr_2$ precursor solution was prepared by dissolving 800 mg of lead bromide ($PbBr_2$) in 2 mL of DMSO. The solution was stirred and heated at 70°C for 30 minutes to achieve complete dissolution. After this step, 600 mg of cesium iodide (CsI) was added, and the mixture was continuously stirred at the same temperature for an additional 30 minutes. This resulted in a uniform and homogeneous precursor solution, ready for thin film deposition.[9]

Thin Film Deposition

A one-step spin-coating method was employed for the deposition of $CsPbIBr_2$ thin films onto the pre-cleaned glass substrates. The spin-coater was set to 6000 rpm for 15 seconds. The prepared $CsPbIBr_2$ solution was dispensed onto the substrate using a dropper, and the spin-coating process was conducted for 15 seconds. This process was repeated to ensure a uniform coating over the substrate surface.[10]

Annealing of Thin Films

After deposition, the thin films were dried in an oven at 60°C for 5 minutes to remove any residual solvent. To enhance the crystallinity and structural quality of the films, they were annealed at different temperatures based on the desired film properties. After annealing, the $CsPbIBr_2$ thin films were stored in sealed containers to protect them from environmental factors and to prepare them for subsequent characterization and analysis.[10]

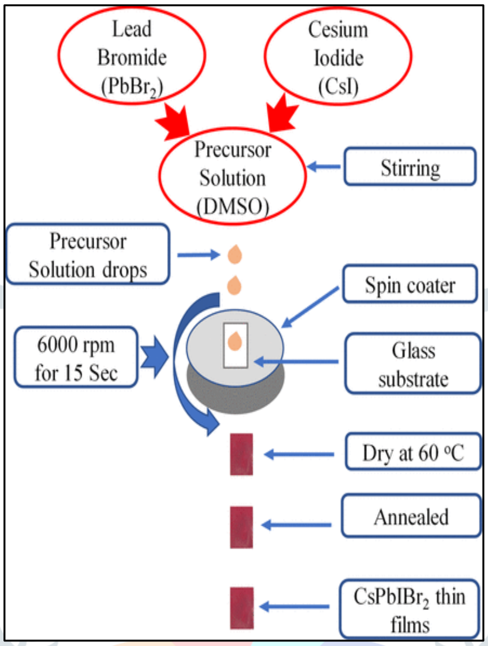

2. RESULTS AND DISCUSSIONS:

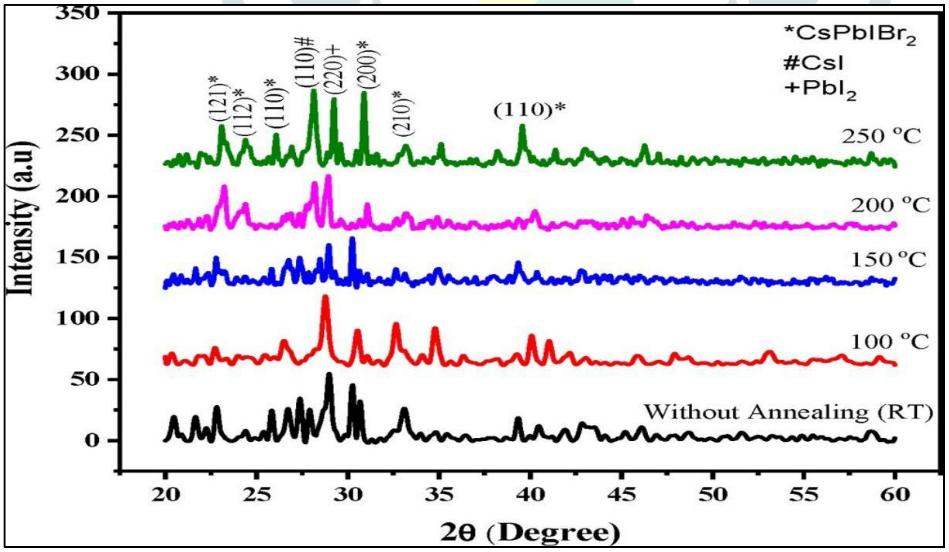

Figure 2 : XRD Analysis of $CsPbIBr_2$ thin films Synthesized under varying annealing Temperatures

XRD Analysis

Figure 1 shows the XRD spectra for $CsPbIBr_2$ films annealed at different temperatures. The spectra reveal sharper peaks at higher temperatures, indicating improved crystallinity.

Table 1: Table presents the XRD Structural parameters of CsPbIBr$_2$ annealed at different temperatures

sample	fwhm (2θ) radian	crystallite size (nm)	interplanar spacing (d) (nm)
CsPbIBr$_2$-1	0.005234	27	0.308
CsPbIBr$_2$-2	0.0045	32	0.31
CsPbIBr$_2$-3	0.002326	62	0.296
CsPbIBr$_2$-4	0.002616	55	0.309
CsPbIBr$_2$-5	0.003101	46	0.317

Structural Parameters

Table 1 lists the structural parameters obtained from XRD analysis, demonstrating that higher annealing temperatures result in larger crystallite sizes and lower FWHM values.

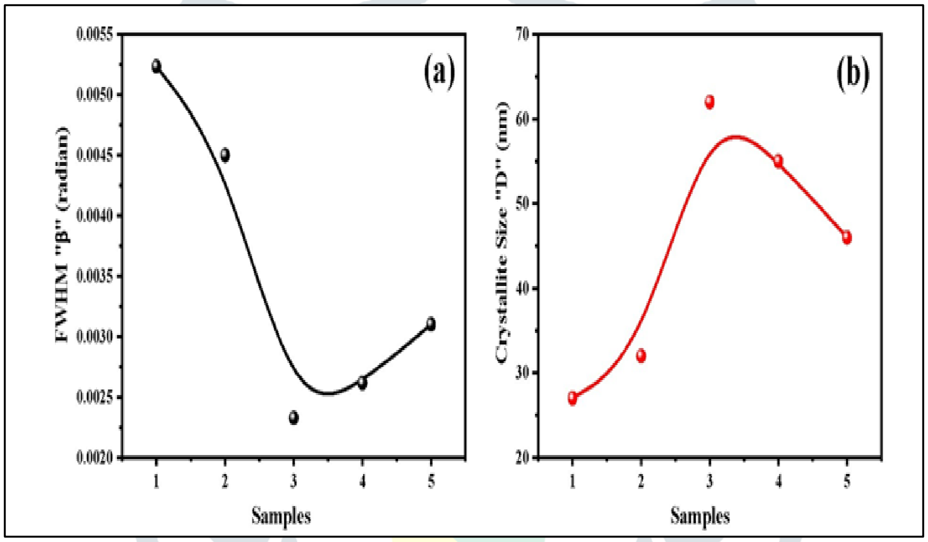

Figure 3: Figure illustrates the dependence of Structural Parameters on Annealing Temperature of CsPbIBr$_2$ thin films: (a) β and (b) D

Graph (a): The FWHM decreases with increasing sample number (annealing temperature), showing a minimum value at sample 4. This is consistent with better crystallization at higher temperatures.

Graph (b): The crystallite size grows with the increase in annealing temperature, reaching its maximum in sample 3, followed by a slight reduction in the subsequent samples.

In summary, the data reveal that annealing temperature has a significant impact on the crystallinity and size of CsPbIBr$_2$ crystallites, with optimal results seen at moderate temperatures around 200°C.

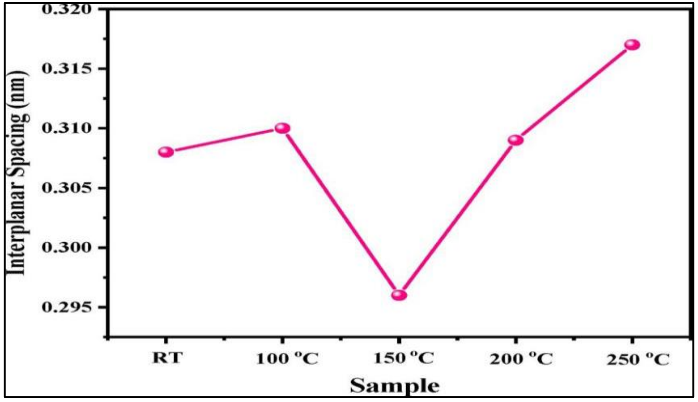

Figure 4: Figure depicts the dependence of interplanar spacing in $CsPbIBr_2$ thin films prepared at various annealing temperatures

The graphs in the image illustrate the morphological and optical properties of $CsPbIBr_2$ thin films annealed at different temperatures.

JETIR

Interplanar Spacing vs. Annealing Temperature:

This graph illustrates the relationship of d-spacing with annealing temperature for the thin films Initially, the interplanar spacing increases slightly between the room temperature (RT) sample and the sample annealed at 100°C. It then drops sharply at 150°C, before increasing again at higher temperatures (200°C and 250°C).

This trend suggests that annealing temperatures influence the lattice structure of the material, with a significant contraction at 150°C, followed by expansion at higher temperatures.

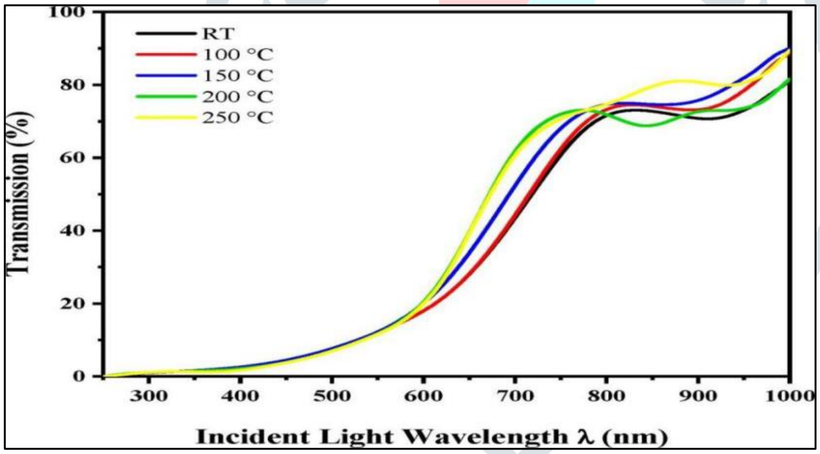

Figure 5: Figure presents the transmission spectra of $CsPbIBr_2$ thin films annealed at various temperatures

Transmission Spectra:

The graph illustrates the transmission spectra percentage of $CsPbIBr_2$ thin films across varying incident light wavelengths (300 nm to 1000 nm) at different annealing temperatures

The transmission increases with wavelength for all samples, with the annealed samples showing a more pronounced transmission in the visible to near-infrared range.

Higher annealing temperatures, particularly 250°C, tend to improve the optical transparency of the films, which is reflected in higher transmission percentages, especially beyond 700 nm.

The optical properties change with annealing temperature, indicating potential optimization of these thin films for light absorption or transparency in specific applications, such as solar cells or optoelectronic devices.

These graphs together demonstrate how annealing temperature affects both the structural (lattice spacing) and transmission properties of $CsPbIBr_2$ thin films

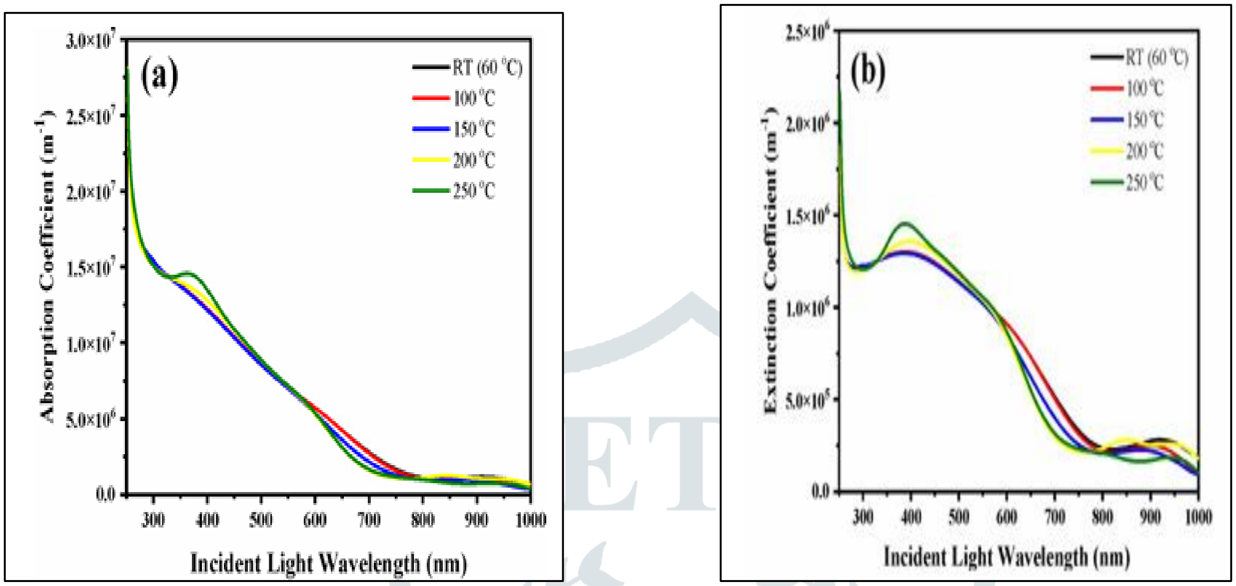

Figure 6: Figure illustrates the Dependence of
(a) The Absorption coefficient and
(b)The Extinction coefficient of $CsPbIBr_2$ prepared at various annealing temperatures

Optical Properties

Figures 4 and 5 presents the transmission spectra and the dependence of absorption/extinction coefficients on annealing temperatures, indicating that higher temperatures enhance the films' optical transparency and reduce light absorption losses.

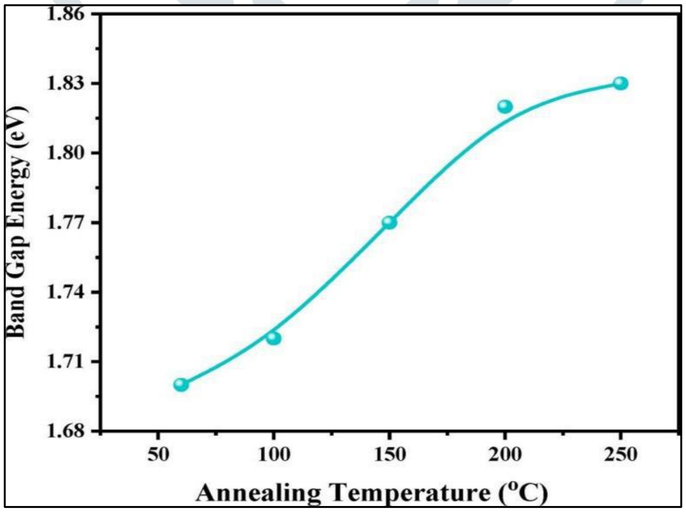

Figure 7: Figure displays the variation in
bandgap energy values of $CsPbIBr_2$
as a function of annealing temperature

Band Gap Energy vs. Annealing Temperature:

Figure 6 shows that the band gap energy increases with annealing temperature, from 1.7 eV at room temperature to 1.83 eV at 250°C, highlighting the improved optical and structural properties with annealing

Table 2: Table presents the bandgap energy of $CsPbIBr_2$ thin films prepared at various annealing temperatures

Samples	Temperature	Band gap energy
1	Room Temperature	1.7
2	100	1.72
3	150	1.77
4	200	1.82
5	250	1.83

Table of Band Gap Energy of $CsPbIBr_2$:

The table presents the band gap values for the samples at various annealing temperatures, indicating that the band gap expands from 1.7 eV at room temperature to 1.83 eV at 250°C. In conclusion, the graphs and data reveal that with rising annealing temperatures, both the absorption and extinction coefficients decline, while the band gap energy increases. These alterations imply that elevated annealing temperatures enhance the optical properties and crystalline quality of the material.

CONCLUSION:

This research underscores the advancements and challenges in PSC technology.

Key achievements include improvements in material stability and efficiency through controlled synthesis and structural optimization. However, issues related to environmental impact, especially lead toxicity, remain critical obstacles for widespread adoption. The study also highlights the potential of lead-free alternatives, which show promise but require further refinement to match the efficiency of lead-based counterparts. Future directions emphasize the need for scalable manufacturing methods and the development of non-toxic, stable materials to enable large-scale, eco-friendly energy solutions. Addressing these challenges will be essential for the commercial viability of PSCs, which could significantly contribute to the global shift toward renewable energy sources.

REFERENCES:

1. Kojima, A., Teshima, K., Shirai, Y., & Miyasaka, T. (2009). Organometal Halide Perovskites as Visible-Light Sensitizers for Photovoltaic Cells. Journal of the American Chemical Society, 131(17), 6050–6051.

2. Yang, W. S., Park, B. W., Jung, E. H., Jeon, N. J., Kim, Y. C., Lee, D. U., ... & Seok, S. I. (2017). Iodide management in formamidinium-lead-halide-based perovskite layers for efficient solar cells. Science, 356(6345), 1376-1379.

3. Grätzel, M. (2014). The light and shade of perovskite solar cells. Nature Materials, 13(9), 838-842.

4. Green, M. A., Ho-Baillie, A., & Snaith, H. J. (2014). The emergence of perovskite solar cells. Nature Photonics, 8(7), 506-514.
5. Saliba, M., Matsui, T., Domanski, K., Seo, J. Y., Ummadisingu, A., Zakeeruddin, S. M., ... & Grätzel, M. (2016). Incorporation of rubidium cations into perovskite solar cells improves photovoltaic performance. Science, 354(6309), 206-209.

6. Jung, H. S., & Park, N. G. (2015). Perovskite solar cells: From materials to devices. Small, 11(1), 10-25.

7. Zhou, Y., Zhao, Y., Zhang, T., Zhang, Y., Zhao, Y., & Yang, M. (2017). All-inorganic $CsPbIBr_2$ perovskite solar cells. Solar Energy Materials and Solar Cells, 173, 324-329.

8. Kim, H. S., Lee, J. W., Yantara, N., Boix, P. P., Kulkarni, S. A., Mhaisalkar, S., & Park, N. G. (2013). High efficiency solid-state sensitized solar cell-based on submicrometer rutile TiO_2 nanorod and $CH_3NH_3PbI_3$ perovskite. Nano Letters, 13(6), 2412-2417.

9. Noel, N. K., Stranks, S. D., Abate, A., Wehrenfennig, C., Guarnera, S., Haghighirad, A. A., ... & Snaith, H. J. (2014). Lead-free organic-inorganic tin halide perovskites for photovoltaic applications. Energy & Environmental Science, 7(9), 3061-3068.

10. Shen, H., Duong, T., Wu, N., Peng, J., Jacobs, D., Gong, J., ... & Weber, K. (2018). Mechanically robust perovskite solar cells with a flexible $CsPbIBr_2$ absorber for long-term stability. Advanced Energy Materials, 8(6), 1701991.